# Formation Mechanism of Boride Nanoparticles by Induction Thermal Plasmas

Takayuki Watanabe[1], Tsuyoshi Ibe[1], Yoshiyuki Abe[2], Yoshiro Ishii[2], Kenji Adachi[2]

[1] *Research Laboratory for Nuclear Reactors, Tokyo Institute of Technology, Tokyo, Japan*
[2] *Central Research Laboratory, Sumitomo Metal Mining Co., Ltd., Chiba, Japan*

**Abstract**
The condensation mechanism of rare-earth boride in thermal plasmas was investigated experimentally. In the thermal plasma, the premixed powder of rare-earth boride with boron was evaporated immediately and nanoparticles were produced through the cooling process. The nucleation temperature of boron, lanthanum and cerium have wide liquid range between the nucleation and melting temperature, resulting in better preparation of boride.

## 1. Introduction

Induction thermal plasmas have been used for production of high-quality and high-performance materials, such as synthesis of nanoparticles, deposition of thin films, plasma spraying and treatments of powders. Induction thermal plasmas have been also applied for treatment of harmful waste materials and recovery of useful material from wastes [1, 2]. These attractive material processes with induction thermal plasmas result from unique advantages; these advantages include high enthalpy to enhance reaction kinetics, high chemical reactivity, large volume with low velocity, oxidation and reduction atmospheres in accordance with required chemical reactions, and rapid quenching ($10^6$ K/s) to produce chemical non-equilibrium materials. These advantages increase the advances and demands in plasma chemistry and plasma processing, such as preparation of various kinds of nanoparticles in metallic and ceramic systems.

The purpose of this paper is to prepare rare-earth boride nanoparticles by induction thermal plasmas. Rare-earth boride is attractive materials because of their high melting temperature, high electrical conductivity and low work function. Therefore these nanoparticles would be applied for the electromagnetic shielding, and solar control windows with interaction with IR and UV light. Some reports about the preparation of boride nanoparticles were published previously; $YB_{66}$ nanoparticles were prepared by plasma chemical process using starting powders of $YB_4$ and B [3]. $TiB_2$ nanoparticles were synthesized in the vapor-phase reaction of sodium with $TiCl_4$ and $BCl_3$ [4].

Another purpose is to investigate the condensation mechanism of mixture vapor of rare-earth metal and boron in thermal plasmas. Investigation of physical and chemical processes in thermal plasma processing is indispensable for production of nanoparticles. Co-condensation process of metal vapors was investigated for Nb-Al and Nb-Si systems [5], Nb-Si and V-Si systems [6]. Formation mechanism was investigated for silicide nanoparticles [7,8]. Vaporization process for Ti-Si, V-Si and Mo-Si systems were also investigated [9]. For nanoparticle preparation with stoichiometric composition, the vaporization and condensation rates of the constituent metals should be controlled in the case of large difference in the vapor pressure.

## 2. Experimental Set-ups

Figure 1 shows a schematic illustration of experimental set-ups for the production of nanoparticle preparation. Induction thermal plasmas were used for preparation of rare-earth bride nanoparticles. The set-ups consist of a plasma torch, a reaction chamber, a

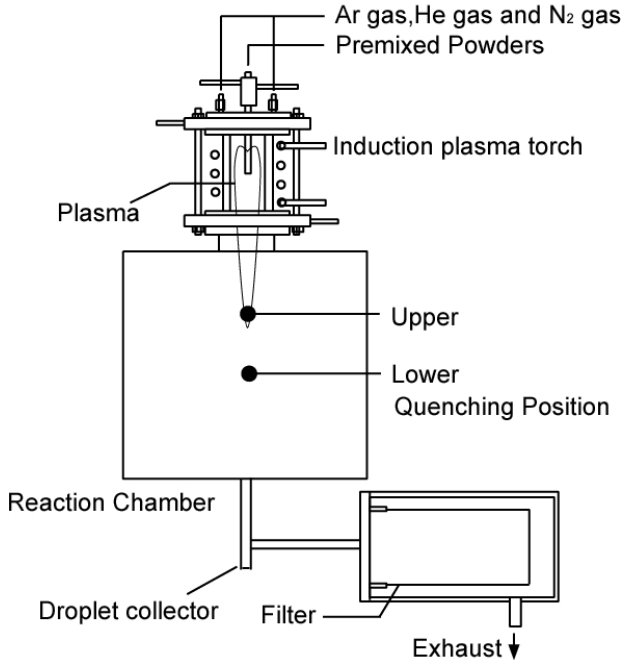


Fig. 1 Experimental set-up for nanoparticle preparation.

prepared particle collection filter and a power supply (4 MHz) at 25 kW. The plasma torch (45 mm i.d., 128 mm length) consists of a water-cooled quartz tube and a working induction coil (3 turn). The reaction chamber was set below the torch. Total system was evacuated and then Ar was introduced up to a pressure of 101 kPa. Premixed powders of $La_2O_3$, B and C were introduced into the thermal plasma from the top of plasma torch at the feed rate of 0.1 g/min. Premixed powders of $La(OH)_3$, B and C were also used for the preparation of $LaB_6$. For the preparation of $CeB_6$, premixed powders of $CeO_2$, B and C were used. Raw material powders used in this study are $La_2O_3$ (average: 14.4 μm), $La(OH)_3$ (average: 1.34 μm), $CeO_2$ (average: 20.2 μm ), B (average: 15.0 μm), and C (average: 1.34 μm). In the thermal plasma, injected powders were evaporated and reacted with boron. After the evaporation and reaction, the vapor was rapidly cooled after the plasma flame. Through the cooling process, metal vapor condensed and boride nanoparticles were produced. The prepared nanoparticles were collected at quenching condition by the water-cooled coil.

The structures of the prepared nanoparticles were determined by X-Ray Diffractometry (XRD, Mac Science MXP3TA). Concentrations of La and B in the prepared particles were determined by Inductively Coupled Plasma Spectrometry (ICP, Seiko Instruments SPS4000), while that of C were measured by Carbon Determinator (LECO EC12). The size distribution of the particles was measured from the photographs of Transmission Electron Microscopy (TEM) for about 1000 particles. TEM observations as well as Electron Diffractometry (ED) were performed on JEOL JEM-2010 operated at an accelerating voltage of 200 kV.

## 3. Experimental Results

### a) La-B-C system

The TEM photograph of the prepared nanoparticles for $La_2O_3$-B-C system was shown in Fig. 2. The particle size distribution shown in Fig. 3 presents the average particles size of 15.0 nm with the geometrical standard distribution of 1.58. The XRD spectrum charts of the prepared nanoparticles for $La_2O_3$-B-C system with the Ar plasma are demonstrated in Fig. 4. $LaB_6$ and $La_2O_3$ were identified from the XRD spectrum peak of the as-prepared particles. The as-prepared particles were separated to nanoparticles in suspension and agglomerated particles in precipitate by ultrasonic dispersion. Nanoparticles are mainly composed of $LaB_6$ with small fraction of $La(OH)_3$ made from $La_2O_3$ at ultrasonic dispersion. The agglomerated particles are identified as $LaB_6$, $La(OH)_3$, $LaBO_3$ with unreacted B from XRD and ED analysis. Induction thermal plasmas provide a powerful tool for the preparation of functional nanoparticles because the phase and composition in nanoparticles can be well controlled.

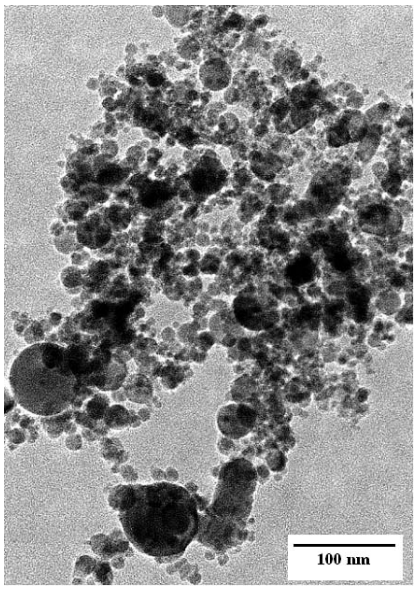


Fig. 2 TEM photograph of nanoparticles for $La_2O_3$-B-C system; $La_2O_3$:B:C = 1:12:3; powder feed rate: 0.1 g/min.

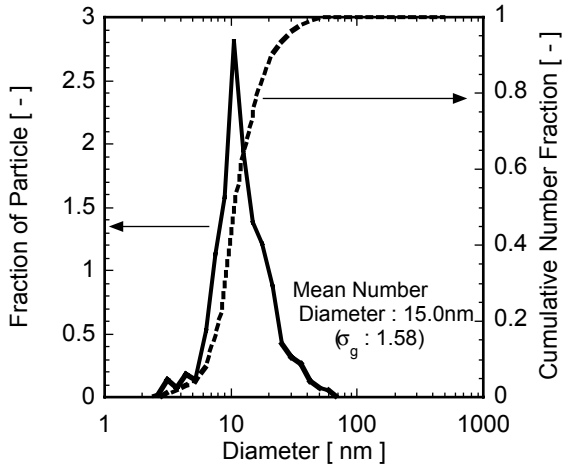


Fig. 3 Particle size distribution for $La_2O_3$-B-C system; $La_2O_3$:B:C = 1:12:3; powder feed rate: 0.1 g/min.

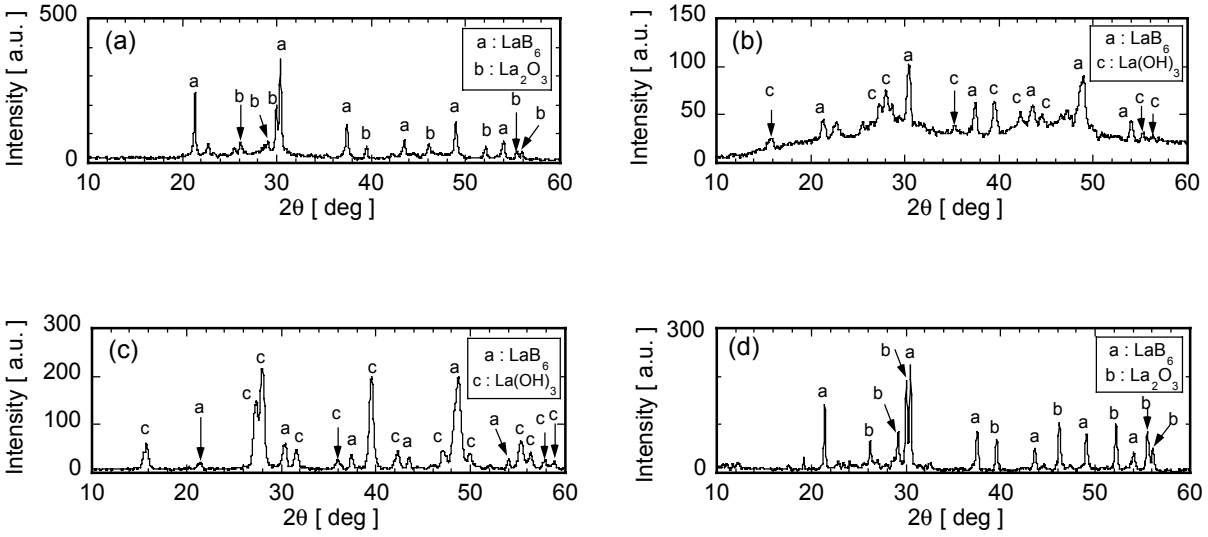


Fig. 4 XRD spectrum charts of nanoparticles for $La_2O_3$-B-C system; $La_2O_3$:B:C = 1:12:3; powder feed rate: 0.1 g/min. (a) as-prepared particles, (b) nanoparticles in suspension, (c) particles in precipitation, (d) unvaporized particles.

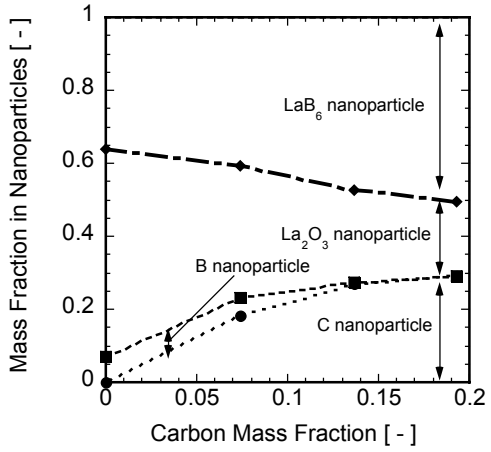


Fig. 5 Effect of carbon mass fraction in the injected powders on the nanoparticle composition for $La_2O_3$-B-C system.

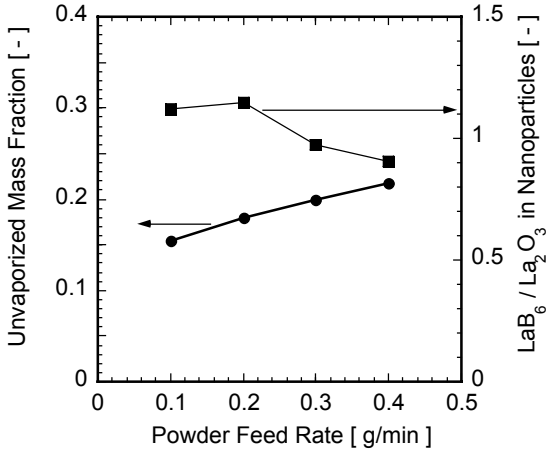


Fig. 6 Effect of powder feed rate on the unvaporized fraction and on the nanoparticle composition for $La_2O_3$-B-C system.

Figure 5 shows effect of carbon mass fraction in the raw powders on the nanoparticle composition. The prepared amount of $LaB_6$ increases with the carbon content, because the injected $La_2O_3$ is easily reduced by carbon in the plasma. Increasing in the carbon content in the feed powder also causes the increase in the carbon content in the prepared nanoparticles. However the carbon in the nanoparticles can be separated by hydrochloric acid treatment; 3 N hydrochloric acid during 20 min at room temperature.

Effect of powder feed rate on the unvaporized fraction of the particles was shown in Fig. 6. The composition of the nanoparticles was also shown in this figure. The unvaporized fraction deceases with a decrease in the powder feed rate, resulting in the enhanced vaporization of boron powders. Therefore the prepared amount of $LaB_6$ nanoparticles are larger at smaller powder feed rate.

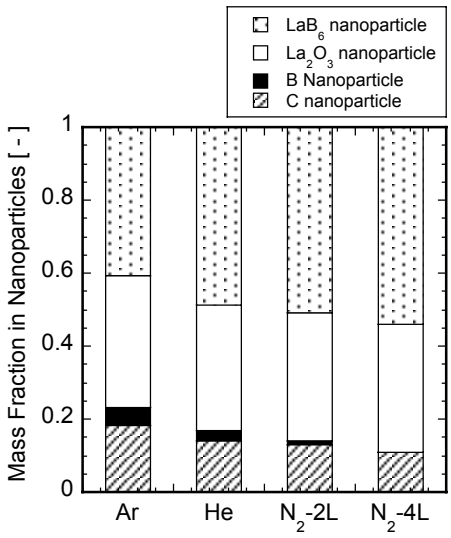


Fig. 7 Effect of plasma gas composition on the nanoparticle composition for $La_2O_3$-B-C system.

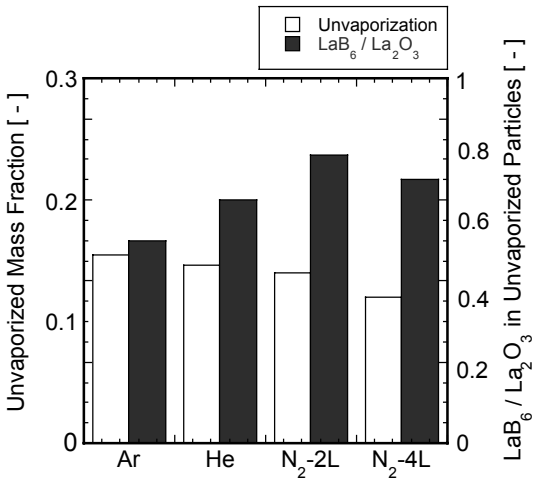


Fig. 8 Effect of plasma gas composition on the unvaporized fraction and on the composition of unvaporized particles for $La_2O_3$-B-C system.

Plasma gas composition has important role on the nanoparticle composition, because the heat transfer rate as well as the reaction mechanism are influenced by the plasma gas composition. Nitrogen (2 or 4 NL/min) or helium (3 NL/min) was added to argon induction plasmas. From the XRD analysis, no peaks due to BN and LaN were not found because ΔG of La nitridation is higher than that of boridation. Effect of plasma gas composition on the nanoparticle composition was shown in Fig.7. Prepared amount of $LaB_6$ nanoparticles were increased by helium or nitrogen plasmas. Addition of helium or nitrogen enhances the heat transfer rate to the injected powders as shown in Fig. 8. The unvaporized fraction of the injected powders is reduced by helium or nitrogen plasma.

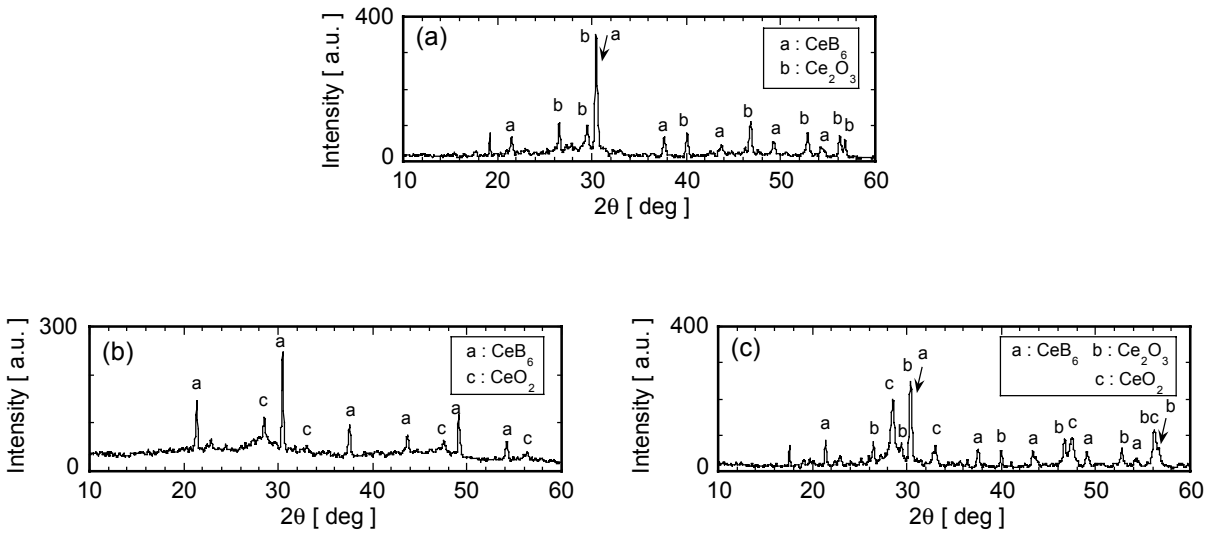


Fig. 9 XRD spectrum charts of nanoparticles for $CeO_2$-B-C system; $CeO_2$:B:C = 1:12:3; powder feed rate: 0.1 g/min. (a) as-prepared particles, (b) nanoparticles in suspension, (c) unvaporized particles.

**b) Ce-B-C system**

The XRD spectrum charts of the prepared nanoparticles for $CeO_2$-B-C system with the Ar plasma are demonstrated in Fig. 9. $CeB_6$ and $Ce_2O_3$ were identified from the XRD spectrum peak of the as-prepared particles. The as-prepared particles were separated to nanoparticles in suspension and agglomerated particles in precipitate by ultrasonic dispersion. Nanoparticles are mainly composed of $CeB_6$ with small fraction of $CeO_2$ made from oxidation of $Ce_2O_3$ at drying.

Figure 10 shows the comparison of nanoparticles composition for $La_2O_3$-B-C and $CeO_2$-B-C systems. The ratio of $LaB_6$ to $La_2O_3$ is larger than the ratio of $CeB_6$ to $Ce_2O_3$ in the as-prepared particles. The better preparation of $LaB_6$ than that of $CeB_6$ is attributed to lower $\Delta G$ of lanthanum boridation than that of cerium boridation.

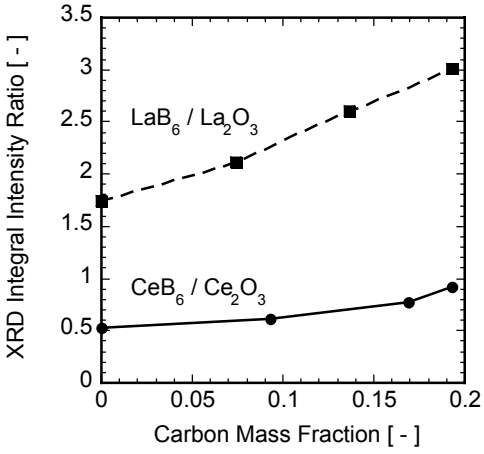


Fig. 10 Comparison of nanoparticle composition for $La_2O_3$-B-C and $CeO_2$-B-C systems.

**4. Discussions**

**a) Vapor pressure**

Vapor pressure difference of boron and rare-earth is the important factor for the controlled composition of the prepared rare-earth boride nanoparticles. The vapor pressure ratio of lanthanum to boron is 13, while that of cerium to boron is 18 at the melting point of born. Small difference in vapor pressure of the constituent components leads to better preparation of boride nanoparticles.

**b) Nucleation Temperature**

Homogeneous nucleation rate has been proposed by Girshick et al. [10]. They derived the expression as an extension of kinetic nucleation theory. The proposed expression can be used over a wide range of physical conditions. Furthermore, the expression for homogenous nucleation, $J$, was consistent with experimental data. Therefore Eq. (1) was used for the estimation of critical saturation ratio.

$$J = \frac{\beta_{ij}\, n_s\, S}{12}\sqrt{\frac{\Theta}{2\pi}}\exp\left[\Theta - \frac{4\Theta^3}{27(\ln S)^2}\right] \tag{1}$$

where $n_s$ is the equilibrium saturation monomer concentration at temperature $T$, $\beta_{11}$ the collision frequency function between monomers, and $S$ the saturation ratio. The dimensionless surface tension $\Theta$ is given by

$$\Theta = \frac{\sigma s_1}{kT} \tag{2}$$

where $\sigma$ is the surface tension, and $s_1$ the monomer surface area. The collision frequency function $\beta_{11}$ can be estimated by Eq. (3) when the Knudsen number is more than 10 [11].

$$\beta_{ij} = \left(\frac{3v_1}{4\pi}\right)^{1/6}\sqrt{\frac{6kT}{\rho_p}\left(\frac{1}{i}+\frac{1}{j}\right)}\times\left(i^{1/3}+j^{1/3}\right)^2 \tag{3}$$

where $\rho_p$ is the particle mass density and $v_1$ the monomer volume. In this model, the particle nucleation is due to the monomer collision, therefore $i = j = 1$.

Relationship between the nucleation rate and saturation ratio is shown in Fig. 11. The nucleation rate is strongly dependent on the surface tension and saturation ratio. When the nucleation rate is over 1.0 $cm^{-3}$ $s^{-1}$, particle formation can be conveniently observed experimentally. Therefore the corresponding value of saturation ratio is defined as the critical saturation ratio [11]. The critical saturation ratio of boron was estimated to be 2, while lanthanum and cerium have the critical saturation ratio of 14 and 16, respectively. Carbon has the highest critical saturation ratio of 42.

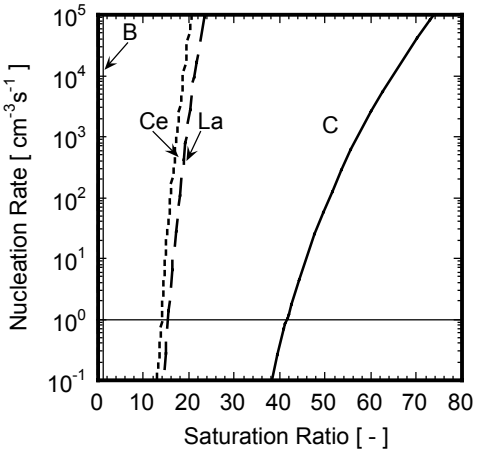


Fig. 11 Relationship between homogenous nucleation rate and saturation ratio for La, Ce, B and C.

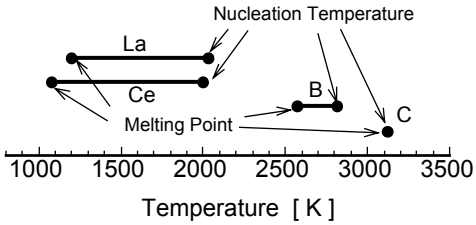


Fig. 12 Nucleation and melting temperature of La, Ce, B and C.

The nucleation temperature at the critical saturation ratio is presented in Fig. 12 for constituent components of boride. The nucleation temperature of carbon corresponds to the melting temperature, while boron, lanthanum and cerium have wide liquid range between the nucleation and melting temperature. The wide liquid range combination of boron with rare-earth metals leads to better preparation of rare-earth boride nanoparticles.

## 5. CONCLUSIONS

Experiments were performed to investigate the condensation of mixture of rare-earth metal with boron in thermal plasmas for the preparation of $LaB_6$ and $CeB_6$ nanoparticles. The nucleation temperature of boron, lanthanum and cerium have wide liquid range between the nucleation and melting temperature, resulting in better preparation of boride. Induction thermal plasmas provide a powerful tool for the preparation of functional nanoparticles because the phase and composition in nanoparticles can be well controlled.

## References

[1] M. Sakano, T. Watanabe and M. Tanaka, *J. Chem. Eng. Japan*, **32**, p.619 (1999).
[2] M. Sakano, M. Tanaka and T. Watanabe, *Thin Solid Films*, **386**, p.189 (2001).
[3] J. Y. Huang, T. Ishigaki, T. Tanaka, S. Horiuchi, *J. Mater. Sci.*, **33**, p.4141 (1998).
[4] R. L. Axelbaum, D. P. Dufaux, and C. A. Frey, *J. Mater. Res.*, **11**, p.948 (1996).
[5] T. Harada, T. Yoshida, T. Kozeki and K. Akashi, *J. Japan Inst. Metals*, **45**, p.1138 (1981).
[6] Y. Anekawa, T. Koseki, T. Yoshida and K. Akashi, *J. Japan Inst. Metals*, **49**, p.451 (1985).
[7] K. Katsuda, T. Watanabe, Y. Abe and Y. Ishii, *Trans. Mater. Res. Soc. Japan*, **27**, p.137 (2002).
[8] T. Watanabe, A. Nezu, Y. Abe and Y. Ishii, *Thin Solid Films, to be published*.
[9] T. Watanabe, H. Itoh and Y. Ishii, *Thin Solid Films,* **390**, p.44 (2001).
[10] S. L. Girshick, C. P. Chiu and P. H. McMurry, *Aerosol Sci. Tech*., **13**, p.465 (1990).
[11] S. K. Friedlander, Smoke, Dust and Haze, John Wiley and Sons (1977).